The magnetic nuclear spin diffusion barrier does it: Polarized proton spin clusters are observed by time-resolved polarized neutron scattering from organic radicals of different size

H. B. STUHRMANN[a,b*]
^aInstitut de Biologie Structurale Jean-Pierre Ebel, CEA/CNRS/UJF, F-38027 Grenoble cedex 1, France
^bHelmholtz-Zentrum Geesthacht, D-21494 Geesthacht, Germany

Motivated by potentially important applications in structural biology, experiments of time-resolved polarised neutron scattering from dynamic polarised proton spin targets were undertaken in order to elucidate the build-up of proton spin polarisation near paramagnetic centres. Organic radicals of different size like EHBA-Cr^V, DPPH and a biradical dissolved in a deuterated solvent were used. These experiments show that an intramolecular proton polarization gradient exists, except for EHBA-Cr^V where it coincides with the radius of its molecular structure. For EHBA-Cr^V, the deuteration of the solvent was varied. In the absence of deuteration, the radius of the radius of the magnetic spin diffusion barrier then appears to fall slightly below 5 Å, the radius of this molecule. Moreover, the characteristic times for the build-up polarized proton spin domains increase dramatically at lower concentrations of EHBA-Cr^V.

1. Introduction

From nuclear magnetic resonance (NMR) spectroscopy, it is well-known that the relaxation of nuclear spins in non-conducting solids is mediated by paramagnetic centres [1]. In a microscopic picture, few spin-1/2 nuclei which happen to be *close* to a paramagnetic centre are relaxed by the fluctuations of the magnetic field of the paramagnetic centres, i.e. the electron spin exchange reservoir (direct relaxation). Their number is limited by the fact that the local spin-lattice relaxation rate is inversely proportional to the sixth power of the distance the nuclear spin and the electron spin. The immediate result is a gradient of nuclear polarisation, which separates the close nuclei subject to fast relaxation from those of the *bulk*, which remain relatively inert. In a second step, the bulk spins are relaxed by diffusion of Zeeman energy to close nuclei. Diffusion among bulk nuclei is an energy conserving process with typical diffusion constant of some hundred nm^2/s for proton spins [2]. This is no longer the case for the close nuclear spins where the Larmor frequencies differ appreciable from those in the bulk of the sample. In the extreme but oversimplified case, the scenario would be the following : i) the close nuclei do not contribute to the signal produced by the other nuclei, ii) in this region the spin diffusion can no longer occur since the total Zeeman energy is not conserved. The point i) may be used to give an estimate of the surface of the spin diffusion barrier by assuming that a flip-flop between neighbouring nuclei would be impossible once their resonance frequency exceeds the width of the NMR profile due to the bulk [3]. The point ii) defines a domain of close nuclei, which differ in their polarisation from that of the other nuclei. A direct observation of the spin diffusion barrier using NMR has been reported by Wolfe [4]. The visualization of this domain is a challenge for structural studies using polarised neutron scattering.

Neutron scattering, and polarized neutron scattering from hydrogen in particular, has all the prerequisites to elucidate the above enigma. The scattering length b of coherent neutron scattering from the nucleus of ^{1}H, the proton, is strongly dependent on the polarisation of the interacting particles [5, 6]

$$b = b_0 \pm b_n P = (-0.374 \pm 1.456\,P)\,10^{-12}\,cm \quad (1)$$

Here a completely polarised neutron beam has been assumed as indicated by $\pm$ for its positive and negative direction with respect to an external magnetic field, respectively. P is the proton polarisation. The large polarisation dependent part b_n of the scattering length of coherent scattering is also the reason for a large cross section of incoherent scattering from protons.

$$\frac{\sigma_{incoh}}{4\pi} = 8.48\left(\frac{3}{4} \mp \frac{1}{2}P - \frac{1}{4}P^2\right)10^{-24}\,cm^2 \quad (2)$$

We note in passing that the scattering length b_0 of the heavier isotope of hydrogen, ^2H, (or deuterium) behaves like that of other nuclei and that its spin dependent part b_n is much smaller than with ^1H, whence its smaller cross section of incoherent neutron scattering.

In order to make neutron scattering experiments operational for structural studies on polarized proton spin domains a high proton polarisation is required, not to mention the polarisation of the neutron beam, which will be close to 1. While the latter is achieved routinely, high values of nuclear polarisation are more difficult to obtain.

For non-conducting hydrogenous material satisfactory results are possible with the method of dynamic nuclear polarisation (DNP) proposed by Abragam [7]. In this case, DNP requires the presence of paramagnetic centres. At temperatures below 1 K and in a magnetic field above 2 T, the electron spin system is almost completely polarised, whereas the nuclear spins are polarised to a fraction of 1%. On irradiation with microwaves of frequency close to the electron paramagnetic resonance (EPR) the polarisation of the electron spin system can be transferred to the nearby nuclei through dipolar interaction between electrons and protons (direct polarisation) that then equilibrates with bulk protons by spin diffusion. The method of DNP allows both positive and negative proton polarisation by choosing a microwave frequency slightly below or slightly above the electron paramagnetic resonance, respectively [8]. Clearly, the close protons are the main players not only in nuclear relaxation but also in dynamic nuclear polarisation.

It is the easy and fast change of the direction of DNP that has been exploited most successfully for the study of the build-up of proton polarisation by time-resolved polarized neutron scattering and simultaneous time-resolved NMR [8, 9, 10]. These experiments show a sharp increase of the intensity of polarized neutron scattering at the onset of DNP due to the close protons and a relatively slow change of the NMR intensity due to the bulk protons. They reflect a fast build-up of the polarisation of the close protons which then in a second step propagates to the other more remote protons of the bulk.

For most of the samples, the radical molecules were dissolved in a deuterated solvent. In the case of the organo-metallic complex of Cr^V, the $(C_{12}H_{20}CrO_7)^-$ anion (abbreviated as EHBA-Cr^V) the 20 hydrogen atoms are inside a sphere of a radius of 6 Å centred at chromium atom. From the analysis of the time-resolved neutron scattering data it appears that the spin diffusion barrier can be identified with the surface of the EHBA-Cr^V molecule [8]. In other words, it is the gradient of isotopic composition, which serves as a spin diffusion barrier. At this point, no conclusions can be drawn about an eventual contribution from a magnetic spin diffusion barrier. These will rely on the study of larger radical molecules in deuterated solvents and on the more difficult neutron scattering experiments using protiated solvents, which are subject of this paper.

2. Experimental

A detailed report on the sample preparation, the cryostat unit, the NMR and microwave system, and on the timing and control of DNP, NMR and neutron data acquisition can be found in Ref. [8,9]. Here, we present experimental details that are necessary on order to achieve a self-contained presentation.

2.1. Sample preparation

Sodium bis(2-hydroxy-2-ehtylbutyrato) oxochromate (V), abbreviated as EHBA-Cr^V, was synthesised from 2-ethyl-2-hydroxybutyric acid and sodium dichromate in dry acetone [11]. The crystals of EHBA-Cr^V were dissolved in a deoxygenated mixture of equal volumes of glycerol and water. Glassy slabs of dimensions 14x14x3 mm^3 were obtained by injecting the solution into a copper mould cooled by liquid nitrogen.

2,2-di(4-tert-octylphenyl)-1-picryl-hydrazyl free radical , loosely abbreviated as DPPH, and deuterated polystyrene beads were dissolved separately in toluene and then combined in the appropriate ratio. The degree of deuteration was lowered by addition of ortho-terphenyl. The solution was allowed to dry and deoxygenated. The solid sample had the dimensions of 14x14x3 mm^3.

A biradical with well-defined, long distance between two unpaired electrons has been synthesized by A. Godt et al. [12]. The sample preparation follows a procedure similar to that used with DPPH.

2.2. SANS measurements

The SANS measurements were performed at the SANS instrument D22 of the Institute Laue Langevin, Grenoble, France, and at the SANS instrument of the Paul-Scherrer Institute (PSI), Villigen, Switzerland. We used polarised incident neutrons of wavelengths λ=4.6 Å with a wavelength spread δλ/λ =0.1 (FWHM). The solid sample were inserted into the NMR coil, placed in a microwave cavity and mounted inside a ^{4}He refrigerator, which was operated at a temperature of about 1 K. A longitudinal static magnetic field of 3.5 T was provided by a superconducting split-coil solenoid. Samples could be changed and cooled down to 1K in less than half an hour.

Two IMPATT-diodes, tuned to frequencies required for positive and negative DNP, of 97.00 GHz and 97.5 GHz, respectively, could be connected to the sample cavity by a wave-guide switch (switching time 100 ms: shut in 5 ms, no microwaves for 90 ms, opened in 5 ms). Continuous-wave (cw) NMR was used in parallel to monitor the bulk proton polarisation. The direction of nuclear polarisation was reversed typically every 5 (or 10) s, and the acquisition of the neutron scattering intensity spectra was triggered synchronously in time intervals of 0.05 (or 0.1) s. Each of the 200 (or 400) time frames was averaged over several thousand cycles (typical counting time 10 hours) to obtain sufficient statistical accuracy. The time dependent scattering intensity was then obtained as

usual by radial averaging and correction for polarisation dependent transmission, and background scattering.

3. The thermodynamic model

The macroscopic aspects of DNP are well understood in the frame of the spin temperature theory [13]. The thermodynamic model assigns heat reservoirs to various degrees of freedom of the electronic and nuclear spin systems that are coupled via mutual and external interactions. The mechanism of DNP then is described as a two-step process: the *cooling* of the non-Zeeman reservoir by a non-saturating microwave field and the subsequent transfer of entropy from the Zeeman reservoir system via *thermal mixing*. It is assumed that this transfer is efficient, so that the spin temperatures of both systems will become equal.

Following this model, the temporal evolution of the close proton polarisation can be described in terms of rate equations governing the flow of polarisation between three (or more) reservoirs coupled in series. There is the electronic spin-spin interaction reservoir *R0* that is cooled by the microwaves, which results in $\left|P_0\right|$ close to 1 pushing the polarisation of the close protons of the non-Zeeman reservoir *R1* in either positive or negative direction depending on the choice of the microwave frequency.
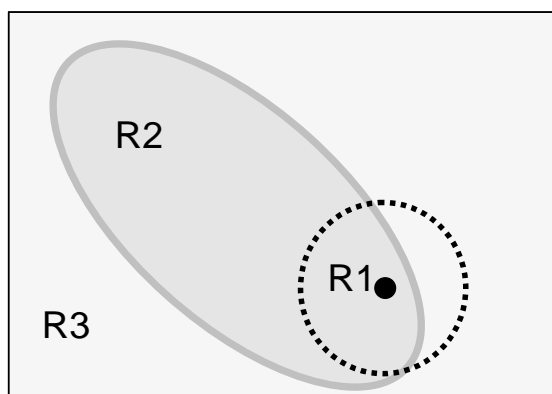

Fig.1. The ellipsoidal protiated molecule is embedded in a matrix R3 that may be deuterated or protiated. The magnetic spin diffusion barrier (broken line) including is assumed by spherical. R1 stands for the non-Zeeman reservoir. The protons of the solute outside R1 constitute R2.

For solutions of organic radical in a deuterated solvent, we define two Zeeman reservoirs *R2* and *R3*. The reservoir *R2* is separated from the reservoir *R1* by a *magnetic* spin diffusion barrier. *R2* contains the protons of the solute outside *R1*. The reservoir *R3* of the deuterated solvent is separated from the reservoir *R2* by an *isotopic* spin diffusion barrier, i.e. by a steep gradient of isotopic composition (Fig. 1). The proton concentration in *R3* is very low, but as the volume fraction of *R3* is high, the total number of protons *R3* may exceed that of the solute.

For the present purpose, we define two cases of a degenerate system.

i) the magnetic spin diffusion barrier may be indistinguishable from the isotopic spin diffusion barrier. We define *R1:=R1+R2*, and then *R2:=R3*.

ii) in the absence of deuteration the proton polarisation in *R2* and *R3* will be the same. We define *R2:=R2+R3*.

3.1. The dynamics of nuclear polarisation

Three rate equations govern the dynamics of the four reservoirs *R0* to *R3* coupled in series.

$$\frac{dP_1}{dt} = \frac{W_{01}}{N_1}\left(P_0 - P_1\right) + \frac{W_{12}}{N_1}\left(P_2 - P_1\right)$$

$$\frac{dP_2}{dt} = \frac{W_{12}}{N_2}\left(P_1 - P_2\right) + \frac{W_{23}}{N_2}\left(P_3 - P_2\right) \quad (3)$$

$$\frac{dP_3}{dt} = \frac{W_{23}}{N_3}\left(P_2 - P_3\right)$$

N_i and P_i denote the number and polarisation of protons belonging to the reservoir *Ri*. The rate constants W_{ij} are defined as probabilities of a mutual spin flip per time unit. The solution of the three coupled linear differential equations in terms of $P_1(t)$, $P_2(t)$ and $P_3(t)$ is obtained by numerical methods simulating the flow of proton polarisation between the four reservoirs.

For the degenerate systems of only three reservoirs $R0$ to $R2$ the terms related to $R3$ in (3) have to be omitted. For this case, the general solution of the set of coupled first order differential equations in terms of $P_1(t)$ and $P_2(t)$ is derived in [10]. The time dependence of the polarisation of the protons in *R1* then is described as a sum of a constant and two exponentials with the time constants τ_1 and τ_2:

$$\tau_{1,2} = \frac{2N_1}{W_{12}\left[1 + w + n \pm \sqrt{\left(1 + w + n\right)^2 - 4wn}\right]} \quad (4)$$

where $w = W_{01}/W_{12}$ and $n = N_1/N_2$. The initial change of the proton polarisation after a reversal of the direction of DNP is mainly described by the short time constant τ_1 whereas the influence of τ_2 extends over a larger time.

3.2. The polarisation dependent neutron scattering intensity

The calculation of the intensity of time-resolved neutron scattering based on a model will take into account three contributions: i) coherent small-angle scattering, ii) incoherent scattering, and iii) background scattering.

$$S(Q,t) = C \left[S_{coh}(Q,t) + S_{incoh}(t) \right] T(t) + S_{background}(Q,t) \quad (5)$$

The factor C takes into account both the way in which the instrument is operated and some properties of the sample. As for the latter the concentration of the radical molecules and the transmission of the sample at P=0 enter into C. T(t) is the time-dependent part of the transmission.

3.2.1 The intensity of coherent scattering

In the absence of nuclear polarisation the amplitude $A(\mathbf{Q})$ of non-interacting particles in dilute solution is given by the difference between $A(\mathbf{Q})_{free}$ of the molecule in vacuo and $A(\mathbf{Q})_{shape}$ of the volume excluded to solvent molecules, i.e. the molecular shape.

$$A_0(\mathbf{Q}) = A(\mathbf{Q})_{free} - A(\mathbf{Q})_{shape} \quad (6)$$

where $\mathbf{Q}$ is the momentum transfer.

In the presence of proton polarisation, we proceed in a similar way: i) we take the known positions of the protons in each Ri, except those of the last one of the series. Their amplitudes of the set of protons in Ri define $B_i(\mathbf{Q})$. ii) We define the region occupied by the same Ri. Its amplitude is $V(\mathbf{Q})$. The polarisation dependent amplitude is

$$A_P(\mathbf{Q},t) = \sum_i P_i(t) B_i(\mathbf{Q}) - P_V(t) V(\mathbf{Q}) \quad (7)$$

where $P_V(t)$ is the proton polarisation of the solvent. Using the expansion of the scattering amplitude as a series of spherical harmonics, we obtain the intensity of coherent small-angle scattering.

$$S_{coh}(Q,t) = 2\pi^2 \sum_{l=0}^{L} \sum_{m=-l}^{l} \left| A_{l,m}^{(0)}(Q) + A_{l,m}^{(P)}(Q,t) \right|^2 \quad (8)$$

where $Q = |\mathbf{Q}| = \dfrac{4\pi}{\lambda} \sin \vartheta$, λ = wavelength and 2ϑ = scattering angle. $S_{coh}(Q,t)$ is the differential cross section of coherent scattering $\sigma_{coh}(Q,t)/4\pi$ of a single molecule in solution.

We remember that the coefficients $A_{l,m}(Q)$ of the expansion of $A(\mathbf{Q})$ as a series of spherical harmonics

$Y_{l,m}(\theta,\varphi)$ are obtained from the polar coordinates of the atoms (or of the grid points defining a region) by the following relation:

$$A_{l,m}(Q) = \sqrt{\frac{2}{\pi}} \, i^l \sum_n b_n \, j_l(Q r_n) \, Y_{l,m}^*(\theta_n, \varphi_n) \quad (9)$$

where j_l are the spherical Bessel functions, and b_n is the scattering length of the n-th atom (or grid point).

3.2.2. The intensity of incoherent scattering

The intensity of incoherent polarised neutron scattering is mainly due to the scattering from protons. The cross section of incoherent scattering $\sigma_{inc.}$ depends on the polarisation P of the protons [5]. We define $S_{inc.}(t)$ as the product of $\sigma_{inc.}$ and the number N of solvent protons attributed to one radical molecule.

$$S_{incoh}(t) = N \frac{\sigma_{incoh}(t)}{4\pi} = 8.48 \, N \left(\frac{3}{4} \mp \frac{1}{2} P(t) - \frac{1}{4} P^2(t) \right) 10^{-24} \, cm^2 \quad (10)$$

With $7x10^{22}$ protons per cm^3 of a frozen mixture of glycerol and water and $5x10^{19}$ unpaired electrons per cm^3, the number of N protons per unpaired electron is $7x10^{22}/5x10^{19} = 1.4x10^3$, for instance. In a highly deuterated solvent, N is lower by two orders of magnitude because of the lower protium concentration.

3.2.3. Background scattering

This category in a large sense includes those contributions of the scattering intensity, which might obscure the data analysis in terms discussed in 3.2.1 and 3.2.2. Some of these contributions are known. The measurement of the neutron scattering intensity of the empty refrigerator together with the variation of the transmission of the sample with the polarisation provides a good estimation of the background scattering intensity. This procedure may be insufficient for the polarisation dependent intensity of the background scattering from the frozen solvent of the sample. Additional correction terms depending on the proton polarisation of the solvent may be needed.

3.3. The NMR intensities

The NMR intensities have been measured simultaneously with the neutron scattering data. Their time resolution is limited to about 1s. Nevertheless, their role in the analysis of the time-resolved neutron scattering data is crucial in many cases. Their importance relies on the fact that they mirror mainly the proton polarisation of the bulk protons. The relatively small contribution of the close protons to the NMR intensity has been discussed by Leymarie [3].

3.4. Comparison of the model.

As the time dependent part of $S(Q,t)$ is small compared to the total intensity, it is convenient to subtract its time average at each Q.

$$Z(Q,t) = S(Q,t) - \frac{1}{T}\int_{t=0}^{t=T} S(Q,t)dt \qquad (11)$$

In this way, we suppress the contribution to $S(Q,t)$ not depending on P to a large extent. The same procedure is applied to the measured time resolved scattering intensity: $S_{exp}(Q,t)$ results $Z_{exp}(Q,t)$.

The difference between the calculated $Z(Q,t)$ and the measured $Z_{exp}Q,t)$ is minimized in an iterative procedure using the scale factor C, the rate constants W_{01}, W_{12} and W_{23} defined in (5) and (3), respectively, and to a minor extent the coefficients describing the background scattering intensity. The extreme values of the proton polarisations measured by NMR are compared with those proposed by the neutron scattering data. Their differences enter into a penalty term. The explicit expression to be minimized is

$$Min = \sum_i \sum_j \left[Z(Q_i,t_j) - Z_{exp}\left(Q_i,t_j\right)\right]^2 + \qquad (12)$$

$$\left[P_{calc}^{NMR,max} - P_{exp.}^{NMR,max}\right]^2 + \left[P_{calc}^{NMR,min} - P_{exp}^{NMR,min}\right]^2$$

The indices i and j refer to the channels of Q and t. Finally, the profile of time-dependent polarisation of the bulk protons obtained from the analysis of the neutron scattering data is compared with that from time-resolved NMR (see section 4.1).

4. Results

Here we summarize results from experiments of time-resolved polarized neutron scattering and NMR from three radical molecules of different size.

4.1. EHBA-Cr^V

The best agreement of the measured time-resolved neutron scattering with the corresponding intensity calculated from the model using (12) is obtained with a spherical diffusion barrier of about 10 Å diameter, which roughly coincides, with the extremes of the molecular structure of the EHBA-Cr^V anion.

18 out of 20 protons of the EHBA-Cr^V molecule appear to be inside the spherical spin diffusion barrier. As the deuterated solvent contains nearly no protons, the isotopic spin diffusion is indistinguishable from a magnetic spin diffusion barrier [8, 9, 10, 14].
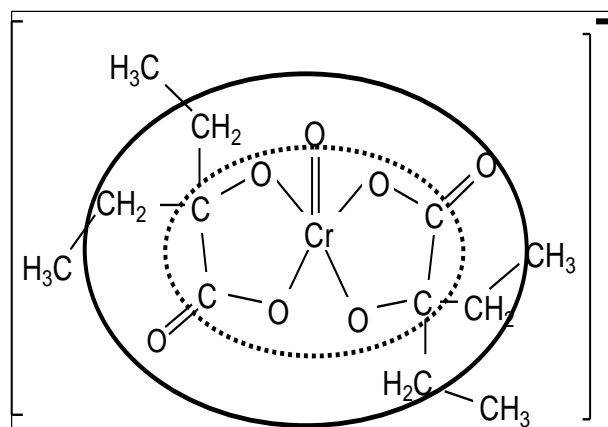

Fig. 2. The molecular structure of EHBA-Cr^V and its proton spin density (————) as observed in the absence of deuteration. The electron spin density (··············) extends to the nearest carbon atoms.

In the absence of deuteration of the solvent, the radius of a spherical spin diffusion barrier of 4.2 Å is slightly smaller than that of EHBA-Cr^V in a deuterated solvent (Fig.2). As there is no gradient of isotopic composition, it is the magnetic spin diffusion barrier, which allows for an enhanced local proton polarisation. There are 9 protons of the solute, mainly those of CH$_2$ groups, and 7 protons of the solvent molecules, which constitute *R1*.

Now we turn to the growth of the local proton polarisation in *R1*. As the system comprises the reservoirs *R0* to *R2*, the build-up of proton polarisation can be described by two time constants τ_1 and τ_2 defined by (4). The initial phase of the polarisation build up will be described by the short time constant τ_1 . On passing from a solvent deuteration of 0.98 to 0.8, we observe a decrease of τ_1 from 1.1 s to 0.4 s. τ_1 reaches 0.3 s in the absence of deuteration.

Contrary to the slow variation of τ_1 with the deuteration of the solvent, we find a strong variation of τ_1 with the concentration c of EHBA-Cr^V (Fig. 3). The short time constant τ_1 varies with 1/c, independently of the deuteration of the solvent.
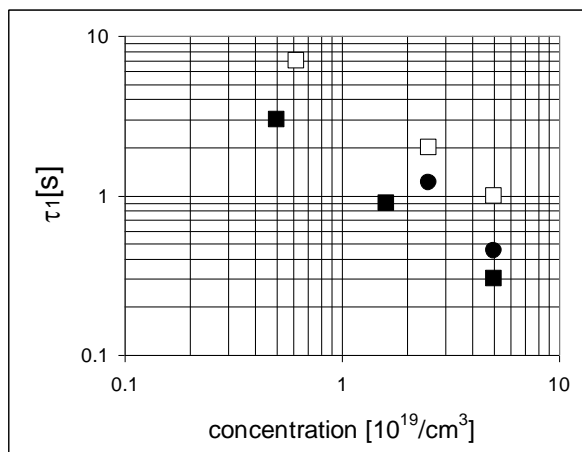
Fig. 3 The short time constant τ_1 versus the concentration of EHBA-Cr^V at various protiation of the solvent: □ 0.02, ● 0.08, ■ 1.

The variation of the proton polarisation in *R2* is obtained from two independent sources: i) time-resolved neutron scattering and ii) from simultaneous measurements of time resolved NMR. The variation of the proton polarisation with time obtained from time-resolved polarised neutron scattering agrees with the corresponding data from time-resolved NMR   (Fig. 4).
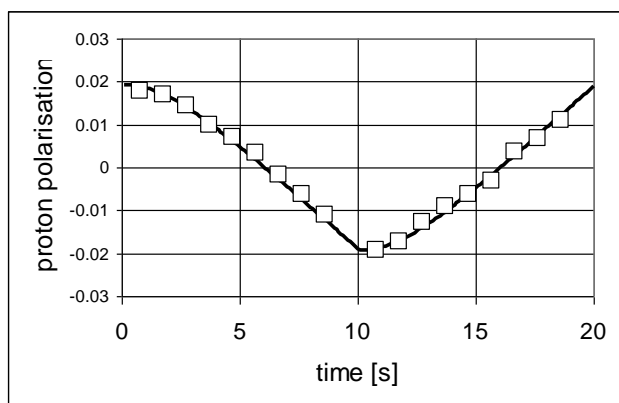

Fig. 4. Comparison of the time-resolved proton polarisation measured by NMR (□) with the proton polarisation of bulk protons obtained from time-resolved neutron scattering (━━━). The sample is EHBA-Cr^V (c= 2.5 x 10^{19} e$^-$/cm^3) in a highly deuterated solvent.

4.2. DPPH in a deuterated solvent

The best agreement of the measured time-resolved neutron scattering of DPPH with the corresponding intensity calculated from the model of DPPH is obtained using a spherical spin diffusion barrier with a radius of about 7 Å. Thus, the reservoir *R1* contains the two-phenyl groups and the picryl group with 10 hydrogen atoms in all and eventually a few hydrogen atoms of the adjacent alkyl groups. The two C_8H_{17} groups with their 34 hydrogen atoms are mostly outside the magnetic spin diffusion

barrier and constitute *R2* (Fig. 5). The hydrogen atoms of the solvent belong to *R3*. This is the result of a number of fits of the experimental data to models using different radii of the magnetic spin diffusion barrier.
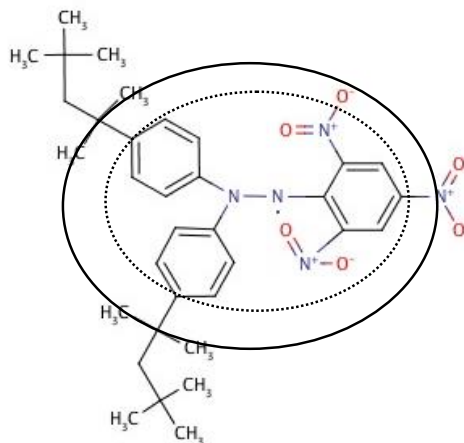

Fig.5. The molecular structure of DPPH and its proton spin density limited by the magnet spin diffusion barrier (━━━). The electronic spin density extends to the phenyl groups (··········).

4.3. A biradical in a deuterated solvent

The molecular structure of the rigid nitroxide biradical is shown in Fig. 5. The best agreement of the measured time-resolved neutron scattering of this biradical with the corresponding intensity calculated from its model is obtained by using spherical spin diffusion barriers with a radius of about 5 Å centred at the $>N-O^\bullet$ groups of each of the pyrroline rings. Each of the two sub-reservoirs of R1 contains 13 hydrogen atoms of the pyrroline ring. The four C_6H_{13} groups with their 52 hydrogen atoms are clearly outside the magnetic spin diffusion barrier and constitute *R2* as shown in Fig. 1a. The hydrogen atoms of the deuterated solvent belong to *R3*.
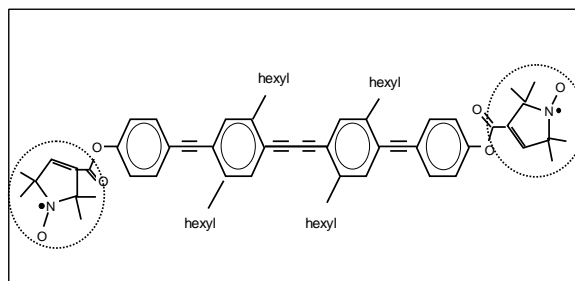

Fig.6. The molecular structure of the biradical and its proton spin density limited by the magnet spin diffusion barrier (············).

5. Discussion

As the polarised unpaired electron acts as a source of proton polarisation it may be argued that its spin density in

the radical molecule in some may defines the contours of the reservoir $R1$. As for the EHBA-Cr^V molecule, the unpaired electron can probably be described in a hybrid p-d function [15]. Its wave function then extends to a certain degree over the neighbouring carbon atoms as it is indicated in Fig. 2.

A more solid statement is possible in the case of DPPH, which has been investigated by both ESR and NMR. Moreover, crystals of DPPH: C_6H_6 have been studied by polarized neutron diffraction [16]. From these and in particular form the latter experiment it appears that there is an important delocalization of the electron spin density over all three rings adjacent to the hydrazyl backbone. The measurable electron spin density extends up to 5Å away from the centre of the N-N bond as it is indicated by a dotted circle in Fig. 6. The magnetic nuclear spin diffusion barrier exceeds the boundary of the electron spin density by 2 Å, only. Thus, the proton spin density map is good probe of the magnetic spin density.

The build-up of proton polarisation proceeds on a time-scale, which depends on the deuteration of the solvent and on the radical concentration. The variation of the proton polarisation as described by (3) then is governed by the transition coefficients W_{ij}. Let us consider the variation of W_{ij} of EHBA-Cr^V with the deuteration of the solvent. Using (12) we limit the analysis to the coefficients W_{01} and W_{12}, i.e. we refer to the three-reservoir model defined by i) in section 3. At high deuteration (low protiation) of the solvent the Ansatz

$$W_{12} \propto c(H_{bulk})^{0.8}$$

(dotted line in Fig.7) provides a good fit of the data [10]. Once the deuteration falls below 0.9, i.e. protiation > 0.1, W_{12} increases only slightly with the protiation of the solvent (Fig. 7). It may be argued that the isotopic barrier is efficient at high deuteration of the solvent and that the magnetic diffusion barrier becomes more important at lower deuteration of the solvent.

The time dependent proton spin density created at the onset of DNP images the electron spin density. As such it temporarily adds an amplitude of the polarised close protons to the existing signal of magnetic neutron scattering of 0.28 10^{-12} cm per unpaired electron. In the absence of deuteration, there will be 17 protons inside a sphere of 8.4 Å diameter. For the most concentrated solution of EHBA-Cr^V the polarisation has been found to vary by 0.21 during one cycle of DNP. The corresponding change of the scattering length is given by the product of the number of close protons - more precisely of their b_n

(see (1)) - multiplied by their polarisation, i.e.
$$\left(17 \times 1.456 \times 10^{-12}\, cm\right) \times 0.21 = 4.95 \times 10^{-12}\, cm$$ (Fig. 8). The scattering length due to the polarised close protons in this case is an order of magnitude larger than the magnetic scattering length of the unpaired electron. At lower concentrations of EHBA-CrV, the gain is even more impressive.
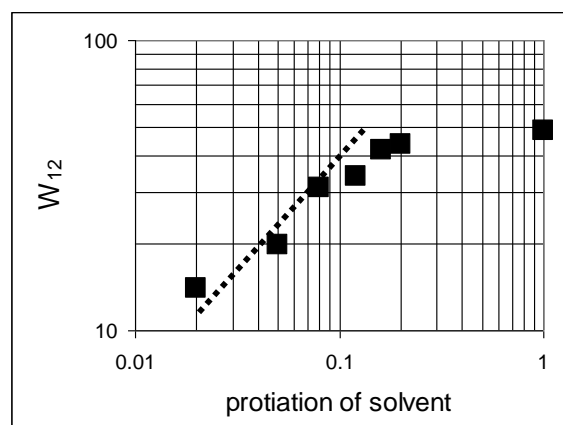

Fig. 7. Transition probabilities versus the protiation of the solvent. ■ W_{12} of EHBA-Cr^V. The dotted line presents the fit at low protiation (see text). The concentration of unpaired electrons is $5 \times 10^{19}\, e^-/cm^3$.
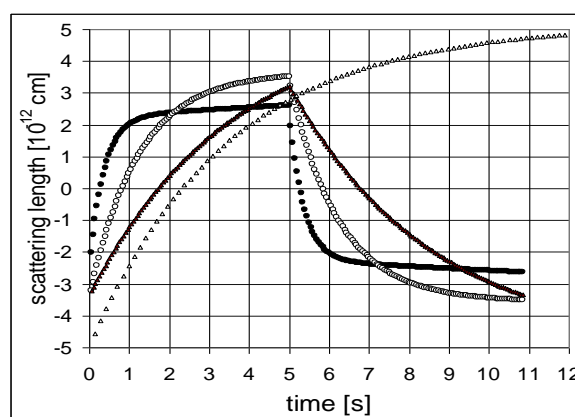

Fig. 8. The variation of the neutron scattering length of the protons close to the Cr^V atom of EHBA-Cr^V in a protiated solvent at three concentrations: 5.0 (●) , 1.6 (○) and 0.5 $10^{19}/cm^3$ (▲) . The scattering length is given in units of 10^{-12} cm. The open triangles simulate the proton polarisation for the lowest concentration of EHBA-Cr^V after prolonged microwave irradiation.

6. Conclusion

Proton spin density created by DNP images electron spin density. Polarised neutron scattering from dynamic polarised proton spin domains adds the dimension of structural resolution to electron paramagnetic resonance (EPR) spectroscopy.

Polarised proton spin domains are fairly strong labels. In the absence of deuteration, their scattering length exceeds that of magnetic neutron scattering by an order of magnitude. In terms of X-ray scattering, the difference between the extremes of the scattering lengths shown in Fig.3 for the lowest concentration of EHBA-Cr^V is equal to the 35 electrons of bromine, which makes it a good label in polarised neutron protein crystallography.

In structural studies using dynamically polarised proton spin domains it is of interest to consider the distance which separate the paramagnetic centres. The distance d between the centres varies with their concentration c like $d \propto c^{-\frac{1}{3}}$. As the fast characteristic time τ_1 varies with 1/c, one obtains $\tau_1 \propto d^3$. In other words, the time needed for the build-up of the local proton spin polarisation in $R1$ increases with the third power of the distance between neighbouring paramagnetic centres. This is another element potentially useful in macromolecular structure research.

The applications of time-resolved polarised neutron scattering from dynamic polarised proton spin domains overlap with those of EPR spectroscopy studies. Spin labelled proteins and membranes and an increasing number of radical proteins, often involved in energy transduction, appear to be promising candidates for future research using **t**ime-resolved **p**roton **p**olarisation (TPP).

Acknowledgements

References

[1] N. Bloembergen, Physica (Utrecht) **15**, 386 (1949).

[2] B. van den Brandt, H. Glättli, P. Hautle, J. Kohlbrecher, J.A. Konter, A. Michels, H.B. Stuhrmann and O. Zimmer, L. Applied Crystallography, 40, s106 (2007).

[3] E. Leymarie, Thèse de doctorat, Université Paris-Sud, N° d'ordre: 7052 (2002)

[4] Wolfe J.P. Phys. Rev. Lett. **31**(15) 907 (1973).

[5] A. Abragam, M. Goldman, Nuclear Magnetism, Order and Disorder, (Oxford: Clarendon) (1982)

[6] H. Glättli, M. Goldman, Methods of Exp. Physiscs, C **23**, 241 (1987).

[7] A. Abragam, Phys. Rev. **98**, 1729 (1955).

[8] B. van den Brandt, H. Glättli, I. Grillo, P. Hautle, H. Jouve, J. Kohlbrecher, J.A. Konter, E. Leymarie, S. Mango, R.P. May, H.B. Stuhrmann, O. Zimmer, Europhys Lett. **59**, 62 (2002).

[9] B. van den Brandt, H. Glättli, I. Grillo, P. Hautle, H. Jouve, J. Kohlbrecher, J.A. Konter, E. Leymarie, S. Mango, R.P. May, A. Michels, H.B. Stuhrmann, O. Zimmer, Nuclear Instruments and Methods A **526,** 81 (2004).

[10] B. van den Brandt, H. Glättli, I. Grillo, P. Hautle, H. Jouve, J. Kohlbrecher, J.A. Konter, E. Leymarie, S. Mango, R.P. May, A. Michels, H.B. Stuhrmann, O. Zimmer, European Phys. J. B **49,** 157 (2006).

[11] M. Krumpolc, J. Rozek, J. Am. Chem. Soc. **101**, 3206 (1979).

[12] A. Godt, C. Franzen, S. Veit, V. Enkelmann, M. Pannier, and G. Jeschke, J. Org. Chem. **65**(22), 7575 (2000)

[13] A. Abragam, M. Goldman, Rep. Prog. Phys. **41**, 395 (1978)

[14] H. B. Stuhrmann, J. Physics, Conference Series, **351,** 012003 (2012)

[15] W. Th. Wenckebach, Proceedings of the Second Workshop on Polarised Target Material, G.R. Court, S.F.J. Cox, D.A. Cragg and T.O. Niinikoski Eds, RL-80-080 (1980) The electronic configuration of Cr(V), p 73

[16] J.X. Boucherle, B. Gillon, J. Maruani, J. Schweizer, Journal de Physique **43**, 12 C7-227 (1982)

---

*Corresponding author: heinrich.stuhrmann@orange.fr